

## Article

# The Difference in Shear Behavior and Strength between Loess and Paleosol and Their Prediction of Unsaturated Strength

Pan Liu <sup>1</sup> , Fuchu Dai <sup>1,2</sup>, Zhiquan Huang <sup>3,\*</sup> and Jiaqi Wu <sup>1</sup>

<sup>1</sup> College of Geosciences and Engineering, North China University of Water Resources and Electric Power, Zhengzhou 450046, China; liupan201498@126.com (P.L.)

<sup>2</sup> College of Architecture and Civil Engineering, Beijing University of Technology, Beijing 100124, China

<sup>3</sup> Luoyang Institute of Science and Technology, Luoyang 471023, China

\* Correspondence: huangzhiquan@ncwu.edu.cn

**Abstract:** In recent decades, loess landslide events have attracted increasing attention in the South Jingyang tableland. To elucidate the mechanical mechanism of landslide initiation in the region, this work collected undisturbed loess and paleosol samples taking from the Q<sub>2</sub> strata in the South Jingyang tableland. A range of direct shear tests were carried out to explore the strength evolution law of shear zone soil subjected to a varying initial moisture content. In addition, soil water characteristic curves (SWCCs) were also charted and used for predicting the unsaturated shear strength. The findings show that the basic physical properties of the paleosol are different from those of loess due to their different pedogenic environments. The normal stress level and initial moisture content jointly determine whether the shear behavior is strain hardening or strain softening. The shear strength and strength parameters evidently diminish with an increasing initial moisture content, and cohesion contributes to the vast majority of strength attenuation. Paleosol samples possess higher values in shear strength and strength parameters than loess samples due to their stronger inter-particle cementation. The predictive formulas of unsaturated shear strength for undisturbed loess and paleosol are proposed, respectively, based on the Vanapalli model, and the calculated values of the strength prediction model are in perfect agreement with the experimental values.

**Keywords:** loess; paleosol; shear behavior; soil water characteristic curve (SWCC); prediction of unsaturated shear strength



**Citation:** Liu, P.; Dai, F.; Huang, Z.; Wu, J. The Difference in Shear Behavior and Strength between Loess and Paleosol and Their Prediction of Unsaturated Strength. *Appl. Sci.* **2024**, *14*, 3301. <https://doi.org/10.3390/app14083301>

Academic Editor: Tiago Miranda

Received: 9 March 2024

Revised: 2 April 2024

Accepted: 3 April 2024

Published: 14 April 2024



**Copyright:** © 2024 by the authors. Licensee MDPI, Basel, Switzerland. This article is an open access article distributed under the terms and conditions of the Creative Commons Attribution (CC BY) license (<https://creativecommons.org/licenses/by/4.0/>).

## 1. Introduction

Loess, a representative, large, porous, weakly cemented, and water-sensitive Quaternary aeolian deposit, is widely distributed in semi-arid and arid regions [1,2]. Paleosol is extensively developed in loess strata and is alternately distributed with loess [3]. The Chinese Loess Plateau is the largest, thickest, and most continuous loess distribution area on Earth [4–6]. Massive numbers of loess geo-hazards (e.g., collapses, sinkholes, landslides, debris flow) have emerged in the Loess Plateau region because of the unique climatic conditions and human engineering activities [7–12], of which loess landslides are extraordinarily prominent [13]. The South Jingyang tableland, in Shaanxi, is famous for high-frequency loess landslide events, and accumulations of strata are deposited in an alternating distribution of loess and paleosol [9,14]. The mechanism of loess landslide occurrence has long been accepted to correlate well with shear strength deterioration of shear zone soil [15,16]. However, gaining a better understanding of the shear behaviors of loess and paleosol with different initial moisture contents is of vital importance for landslide mechanism analysis in the South Jingyang tableland.

To date, the shear characteristics of loess have been widely investigated, and these rich research findings reveal that loess under a dry condition has eminent shear strength; however, in wet environments, the shear strength is prone to a dramatic decline due to the

destruction of inter-particle cementation [17–22]. Similar research results have also been reported in other loess regions abroad. Hadzi-Nikovic et al. [23] studied the strength of loess deposited in Belgrade, and showed a decrease in shear strength owing to greater initial moisture. Yates and Russell [24] conducted triaxial tests to investigate the underlying causes of frequent rainfall-triggered slope failures in the Akaroa harbor area in Banks Peninsula, New Zealand, and the stress–strain curves showed an increase in maximum deviatoric stress as moisture decreased. These plentiful research results offer in-depth insights into the shear behavior of loess, but there remains little investigation of paleosol shear strength. Moreover, the limited research on the paleosol mainly focuses on environmental or paleoclimatic changes [25–27]. However, the existing research has proven that loess and paleosol are different with respect to physical and mechanical properties [16,28]. Consequently, it is essential to conduct a comparative analysis of the strength evolution laws for undisturbed loess and paleosol under different moisture content conditions.

Establishing an effective strength prediction model can provide a good approximation of shear strength for unsaturated soil in the absence of experimental data. Past studies have stated that the SWCC is a critical parameter for estimating the unsaturated shear strengths of soils [29,30]. The prediction of loess shear strength has also made gratifying progress. Zhai et al. [30] proposed a new model for estimating unsaturated shear strength on the basis of the SWCC. Cai et al. [31] established a shear strength formula with matrix suction as a variable. An equation using the SWCC to predict the unsaturated shear strength of loess over a wide suction range was also proposed by Jiang et al. [32]. The results obtained from these strength prediction formulas have good consistency with the measured strength, and they are convenient to apply in engineering practice. However, in our review of the existing literature, we found that there are abundant shear strength prediction models for unsaturated loess, but the research on prediction models for the paleosol is insufficient. Further research is, therefore, needed to establish an effective prediction formula for paleosol shear strength.

This paper clarifies the shear strength deterioration mechanisms of undisturbed loess and paleosol with various initial moisture contents by systematically investigating their shear performance and SWCCs. Furthermore, a theoretical model for predicting the unsaturated shear strength of loess and paleosol is established. The experimental research results hopefully serve as useful information for understanding the shear behavior and predicting the strength of unsaturated loess and paleosol.

## 2. Experimental Details

### 2.1. Sampling and Preparation of Samples

The samples tested were acquired from the South Jingyang tableland (Figure 1), a site that has suffered a considerable number of landslide disasters since 1984 [33]. Field investigations evidenced that the vast majority of sliding surfaces were located between a loess layer and paleosol layer [28,34]. Hence, samples of loess and paleosol were obtained to study their shear properties.

Undisturbed bulk samples of loess ( $L_2$  layer) and paleosol ( $S_2$  layer) with a size of  $200 \times 200 \times 200 \text{ mm}^3$  were collected, and the top sides of samples were clearly marked in the field. Thereafter, they were well sealed with plastic wrap and carefully transported to the laboratory to avoid any disturbance. In the laboratory, these samples were cut using ring knives to a diameter of 63.5 mm and height of 25.4 mm for direct shear tests. The diameter and height of the samples used for charting SWCCs were 61.8 mm and 20 mm, respectively. For the direct shear tests, loess and paleosol samples with initial moisture contents of 11, 13, 17, 21, 26, and 33% (by weight) were prepared by air drying or spraying distilled water. Afterwards, they were wrapped with plastic wrap and placed in an airtight moisturizing container for at least 48 h to achieve water homogenization. It is worth mentioning that samples used for measuring SWCCs should be fully saturated with degassed water before the test begins.

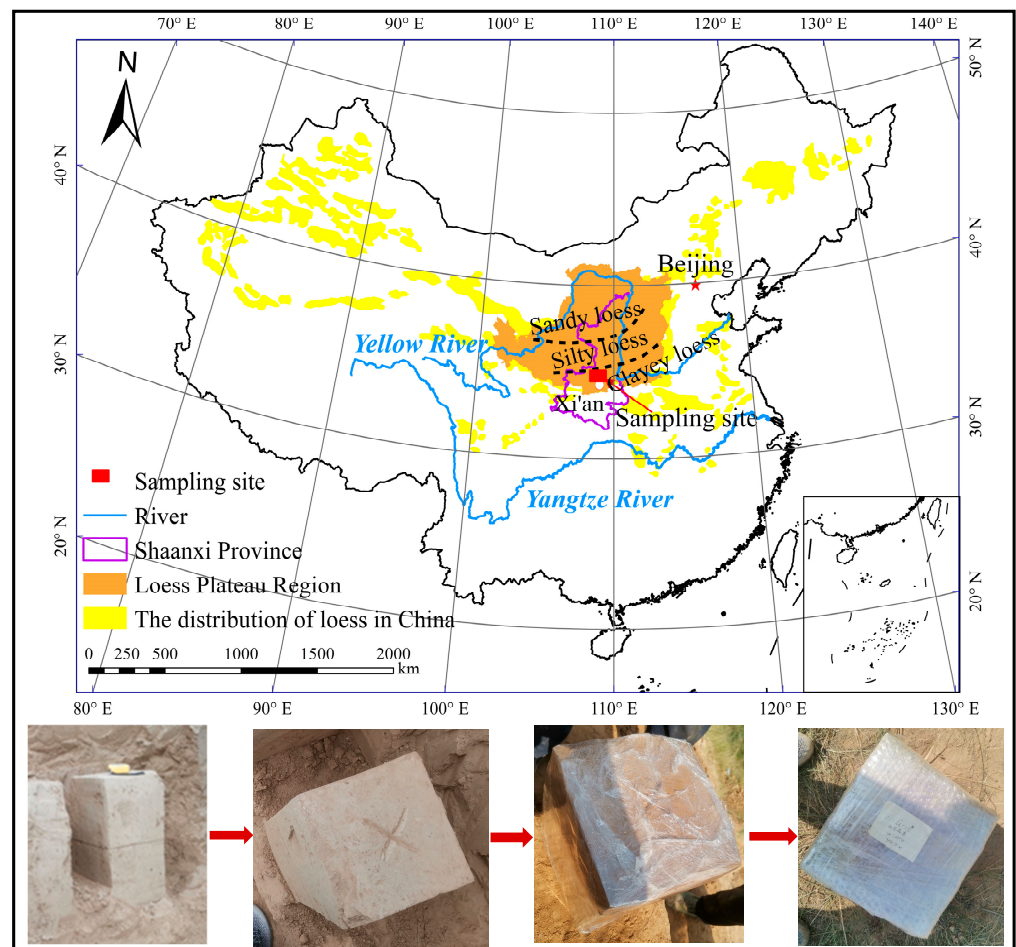


Figure 1. The location and acquisition process of samples (modified according to [4,35,36]).

Loess and paleosol samples' basic physical properties were determined in accordance with the Chinese National Standards (CNS) GB/T50123-2019 [37]. The grain size distributions, measured using a laser particle analyzer (Bettersize2600E), revealed that the loess and paleosol samples were predominantly composed of silt particles with proportions of 79.99~80.21% and 81.89~82.93%, respectively. Their physical properties are presented in Table 1. It can be seen that the paleosol samples had a higher dry density, moisture content, Atterberg limit, and silt and clay contents than the loess samples, and yet their specific gravity and sand content were lower than those of the loess samples. An X-ray diffraction test was implemented to analyze their mineral compositions, indicating that the two soils predominantly incorporated quartz, feldspar, and calcite, with small amounts of chlorite, illite, and amphibole (Table 2). The finding that the carbonate mineral content in the loess samples was higher than that in the paleosol samples (18.7% and 14.4%, respectively) agreed with the findings of the investigation by Yuan et al. [28].

Table 1. Physical properties of loess and paleosol samples.

Sample	$G_s$	$\rho_d/(g/cm^3)$	$w/%$	Atterberg Limits			Grain Size Distribution/%		
				$w_L/%$	$w_P/%$	$I_P$	Sand > 0.05 mm	Silt 0.002~0.05 mm	Clay < 0.002 mm
Loess	2.71	1.49	13.4	29.6	17.0	12.6	11.20~11.49	79.99~80.21	8.52~8.59
Paleosol	2.67	1.51	17.9	31.8	18.3	13.5	3.18~3.80	81.89~82.93	13.89~14.44

Note:  $G_s$ , specific gravity;  $\rho_d$ , dry density;  $w$ , natural moisture content;  $w_L$ , liquid limit;  $w_P$ , plastic limit;  $I_P$ , plasticity index.

**Table 2.** Mineral compositions of loess and paleosol samples.

Sample	Components/%					
	Quartz	Feldspar	Calcite	Chlorite	Illite	Amphibole
Loess	52.3	14.8	18.7	8.4	4.9	0.9
Paleosol	54.1	16.3	14.4	9.9	5.3	/

## 2.2. Testing Program

Usually, one of two methods is used to determine the shear strength of unsaturated soil. One method is to use a direct shear instrument or triaxial equipment, which employs axial translation technology to control suction [20,38]. Although this method has high accuracy, it is difficult to widely apply in engineering practice owing to its slow shear rate, long testing period, and high operating cost. Instead, the combined methods of suction measurement and a conventional direct shear test are widely accepted in practice [39,40]. The related research literature has demonstrated that the results obtained by the two methods are near-identical [41]. That is, the shear strength of unsaturated soil determined by conventional direct shear tests already implies the contribution of matric suction. Based on this, the latter method is introduced to survey the shear behavior of undisturbed loess and paleosol samples under various initial moisture contents.

A fully automatic direct shear apparatus was employed to perform direct shear tests with a maximum shear displacement of 10 mm. Its shear rate in the process of testing was set to 0.2 mm/min, which can be considered a drainage test [42]. The normal stresses of 50 kPa, 100 kPa, 200 kPa, and 400 kPa were imposed during the direct shear test.

The SWCC was measured by the pressure membrane instrument method in this work. For each soil sample (i.e., loess and paleosol), suctions of 20 kPa, 40 kPa, 60 kPa, 80 kPa, 100 kPa, 150 kPa, 200 kPa, 250 kPa, 300 kPa, 390 kPa, and 480 kPa were applied in sequence, respectively. After each level of suction balance, the mass of the soil sample was weighed until the final suction level was reached.

## 3. Results

### 3.1. Shear Behaviors of Loess and Paleosol Samples

The outcomes of the direct shear tests for loess and paleosol samples are illustrated in Figures 2 and 3, respectively. Under this experimental condition, whether the shear stress–shear displacement curve belongs to strain softening or strain hardening depends not only on normal stress but also on the initial moisture content. As the initial moisture content and normal stress increase, their shear failure behavior gradually transitions from strain softening to strain hardening. For loess samples, when the initial moisture content is smaller than 17% and the normal stress is 50~100 kPa, the shear stress–shear displacement curves are of strain softening, and as the normal stress increases to 400 kPa, their curves under an identical initial moisture content gradually transition to strain hardening. Moreover, under a state of a high initial moisture content, they exhibit strain hardening characteristics even with a low normal stress. The shear behavior of paleosol samples is consistent with that of loess samples, and yet the strain softening phenomenon is more notable when compared with loess samples.

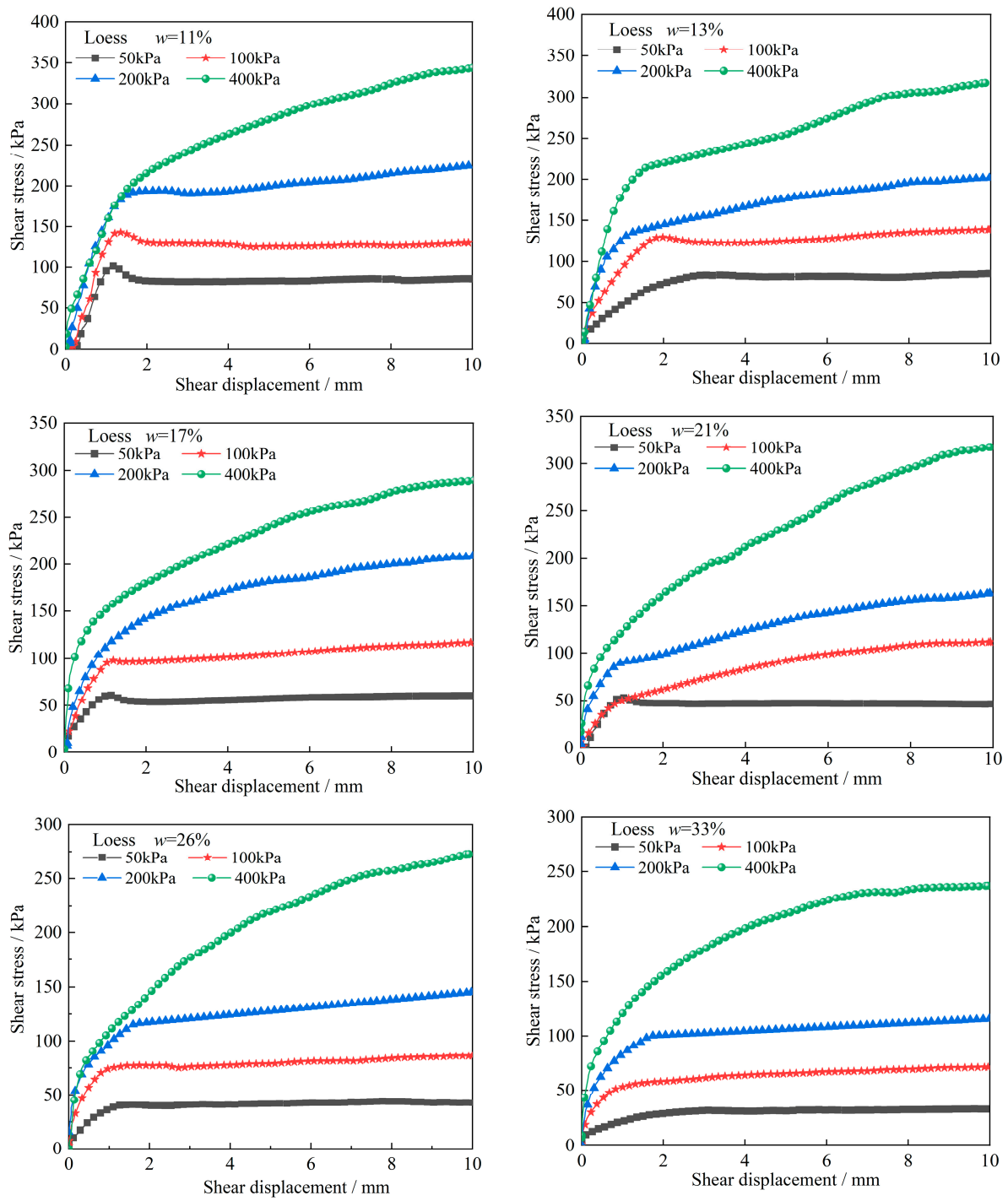
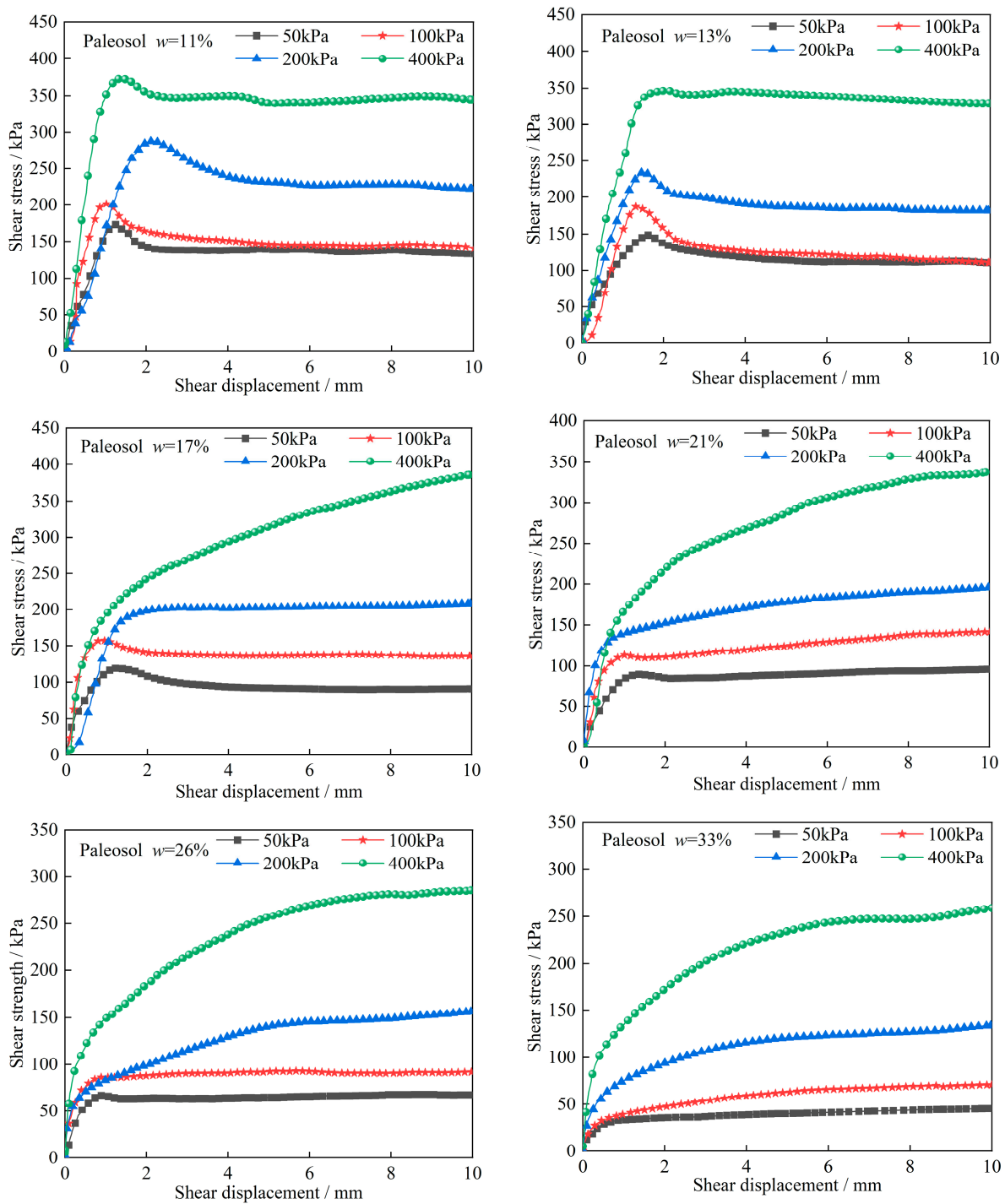


Figure 2. Curves of shear stress versus shear displacement for loess samples.



**Figure 3.** Curves of shear stress versus shear displacement for paleosol samples.

### 3.2. Shear Strengths of Loess and Paleosol Samples and Their Strength Parameters

In line with the Chinese National Standards (CNS) GB/T50123-2019 [37], the peak strength on the shear stress–shear displacement curve is defined as the shear strength. For curve without a peak value, the shear stress at the point where the shear displacement is equal to 20% of samples’ height (e.g., 5 mm of shear displacement) is defined as the shear strength. Figure 4 exhibits their shear strength envelopes with different moisture contents. The shear strength decreases as the normal stress decreases and the initial moisture content increases. For loess samples, when the normal stress is 200 kPa, the increase in the initial water content clearly reduces the shear strength (199.2 kPa at 11% and 106.2 kPa at 33%,

respectively). This means water has a weakening effect on the shear strength of loess. When the initial moisture content rises from 11% to 21%, the shear strength at 200 kPa of normal stress decreases from 199.2 kPa to 134.6 kPa, with a reduction magnitude of 32.4%, whereas it is 21.1% when the initial moisture content increases from 21% to 33% (134.6 kPa and 106.2 kPa, respectively), indicating that the softening effect of water on shear strength is more pronounced at a low initial moisture content than at a high initial moisture content. The same variation trend is seen for paleosol samples, but those have a higher shear strength than loess. The reduction magnitudes of shear strength at the normal stress of 200 kPa are 38.2% and 31.8% when the initial moisture content is increased from 11% to 21% and from 21% to 33%, respectively. This suggests that the paleosol is more sensitive to water than loess.

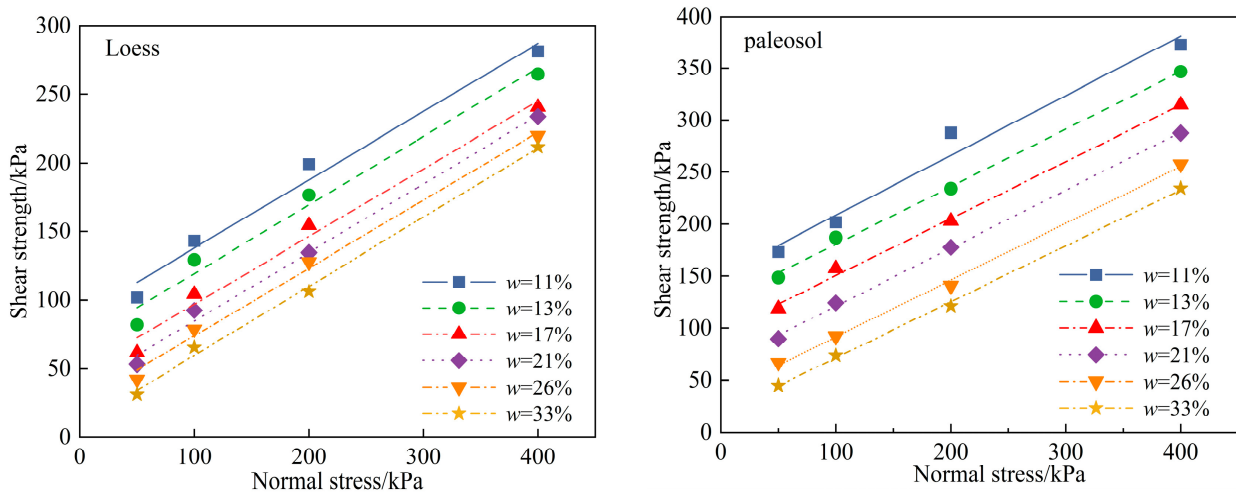


Figure 4. Shear strength envelopes of samples with different initial moisture contents.

Their shear strength parameters are listed in Table 3. We can understand from these that  $c$  evidently decreases with an increased initial moisture content. When the initial moisture content increases from 11% to 33%, the  $c$  of loess and of paleosol is reduced by 89.7% and 88.4%, respectively. Compared with  $c$ ,  $\varphi$  shows a decreasing trend as a whole, but its reduction amplitude does not show large variation. This demonstrates that the weakening effect of water against shear strength is largely reflected in a reduction in  $c$ . In conducting a comprehensive investigation of the relationship between  $c$  and the initial moisture content, we found, when fitting the data in Table 3, that  $c$  decreased exponentially with an increased initial moisture content (Figure 5). Similar results have also been published in the relevant literature [20].

Table 3. Shear strength parameters of loess and paleosol.

Sample	Strength Parameter	Initial Moisture Content/%					
		11	13	17	21	26	33
Loess	$c$ (kPa)	88.2	69.6	47.7	34.7	24.3	9.1
	$\varphi$ (°)	26.4	26.5	26.2	26.5	26.3	26.1
Paleosol	$c$ (kPa)	151.1	125.4	95.8	65.3	37.1	17.6
	$\varphi$ (°)	29.9	28.9	28.7	29.1	28.6	28.3

Note:  $c$  is cohesion;  $\varphi$  is internal friction angle.

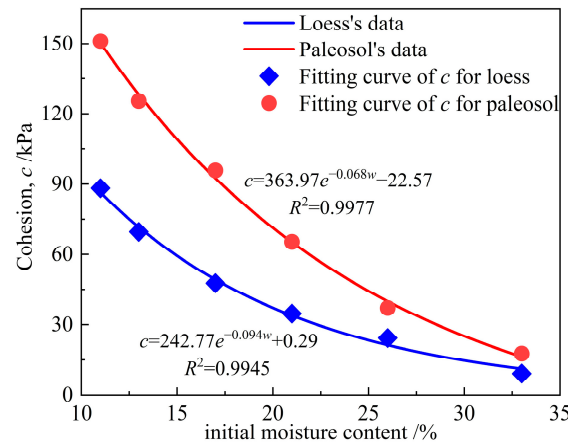


Figure 5. Relationship between cohesion and initial moisture content.

### 3.3. SWCCs of Loess and Paleosol Samples

Figure 6 shows the corresponding data points of the volume moisture content and matrix suction derived from experimentation. To quantitatively characterize the SWCC characteristics, the Van Genuchten (1980) model was employed to fit the data points, according to

$$\theta = \theta_r + (\theta_s - \theta_r) / [1 + (\alpha s)^n]^m \tag{1}$$

where  $\theta$  is the volume moisture content,  $\theta_s$  is the saturated volume moisture content,  $\theta_r$  is the residual volume moisture content,  $s$  is matrix suction,  $\alpha, m, n$  are fitting parameters given in Table 4, and  $R^2$  is the fitting coefficient.

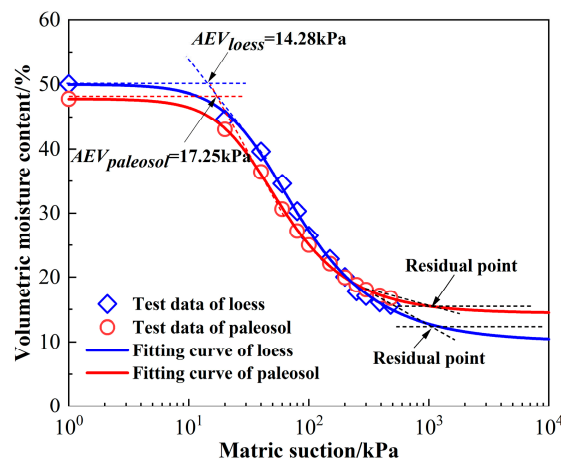


Figure 6. SWCCs of loess and paleosol samples (note that the AEV is the air entry value).

Table 4. Fitting parameters of SWCC model for loess and paleosol.

Sample	Fitting Parameters Based on VG Model					$R^2$
	$\alpha$	$n$	$m$	$\theta_s$	$\theta_r$	
Loess	0.0358	2.1561	0.5362	0.5007	0.1029	0.9976
Paleosol	0.0292	2.0102	0.5026	0.4780	0.1439	0.9996

As can be seen from Figure 6, the higher the  $\theta$ , the smaller the  $s$ . And yet their SWCCs' shapes are quite different due to their varying textures. The  $\theta_s$  of loess is higher than that of the paleosol. This could be attributed to the superior compactness of the paleosol compared to loess ( $\rho_{d,loess} = 1.49 \text{ g/cm}^3$ ,  $\rho_{d,paleosol} = 1.51 \text{ g/cm}^3$ ). As  $s$  grew, the  $\theta$  of the paleosol exceeded that of loess under the same  $s$ , revealing that the paleosol had a stronger water-holding capacity.

### 3.4. Shear Strength Prediction of Loess and Paleosol Samples

The calculation of the shear strength for unsaturated soil, generally, consists of two parts: the saturated shear strength and the shear strength contributed by suction. A shear strength prediction model (Equation (2)) was proposed by Vanapalli et al. [43] based on Canadian glacial till. However, Gao et al. [40] found that Equation (2) was not suitable for direct use on loess because its shear strength was greatly underestimated. So, they added a correction coefficient ( $g$ ) to Equation (2) and thereby produced a shear strength expression (Equation (3)) applicable to loess.

$$\tau_f = c' + (\sigma - u_a) \tan(\varphi') + (u_a - u_w)\Theta^\kappa \tan(\varphi') \tag{2}$$

$$\tau_f = c' + (\sigma - u_a) \tan(\varphi') + (u_a - u_w)(g \cdot \Theta^\kappa) \tan(\varphi') \tag{3}$$

where  $c'$  and  $\varphi'$  are strength parameters of saturated soil;  $(\sigma - u_a)$  is normal stress; for a conventional direct shear test under atmospheric pressure,  $u_a = 0$ ;  $u_w$  is the pore-water pressure;  $(u_a - u_w)$  is matric suction;  $\Theta$  is the relative volume moisture content,  $\Theta = \theta_w / \theta_s$ ;  $\kappa$  is the fitting parameter; and  $g$  is the correction coefficient.

The unsaturated shear strength formulas of loess and paleosol were established by fitting Equation (3) with the experimental data at a normal stress of 200 kPa. The shear strength parameters and fitting parameters in Equation (3) are shown in Table 5. Finally, their unsaturated shear strength formulas are

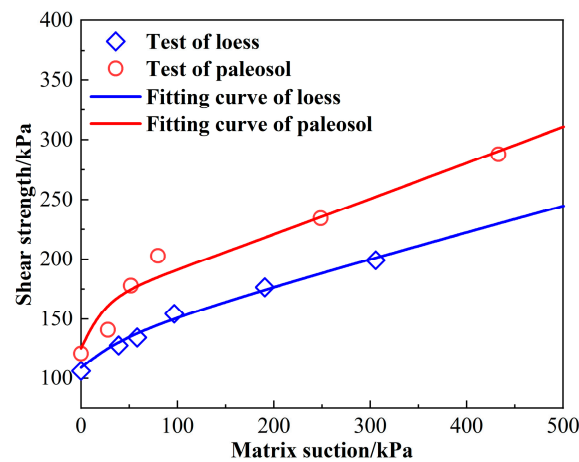
$$\tau_{f,loess} = 9.1 + \sigma \tan 26.1^\circ + 1.29(u_a - u_w)\Theta^{0.72} \tan 26.1^\circ \tag{4}$$

$$\tau_{f,paleosol} = 17.6 + \sigma \tan 28.3^\circ + 2.96(u_a - u_w)\Theta^{1.39} \tan 28.3^\circ \tag{5}$$

**Table 5.** Parameters in Equation (3) for loess and paleosol samples.

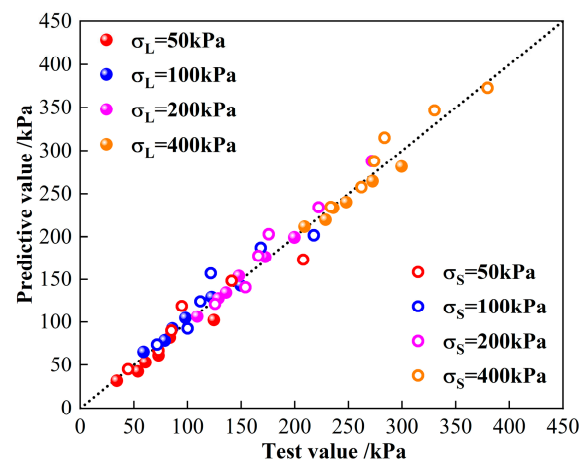
Sample	$c'/\text{kPa}$	$\varphi'/^\circ$	$g$	$\kappa$	$R^2$
Loess	9.1	26.1	1.29	0.72	0.991
Paleosol	17.6	28.3	2.96	1.39	0.960

Figure 7 manifests the relationship between shear strength from the conventional direct shear test and matrix suction after shearing. The excellent fitting degrees (0.991 and 0.960, respectively) verified their accuracy and the suitability of Equations (4) and (5) in describing the relationship between shear strength and matrix suction for unsaturated loess and paleosol.



**Figure 7.** Relationship between shear strength and matrix suction.

To verify the applicability of Equations (4) and (5) and the accuracy of the parameters in the prediction models, the unsaturated shear strength models were verified for various shear strengths from conventional direct shear tests with different normal stresses and initial moisture contents. A comparison of tested and predictive values is depicted in Figure 8, showing that the results are well-distributed near the standard line. Furthermore, SPSS version 19 software was used for significance analysis using the paired *t*-test with a critical level of  $\alpha = 0.05$ . The significance evaluation of the predictive models for loess and paleosol produced results of 0.061 and 0.088, respectively (both greater than 0.05). These can be regarded as demonstrating that there was no significant difference between predictive values and test values. So, we have reason to believe that Equations (4) and (5), determined based on the Vanapalli model, can well predict the unsaturated shear strength of undisturbed loess and paleosol.



**Figure 8.** Comparison of test and predictive shear strengths for unsaturated loess and paleosol (note that the subscripts L and S denote loess and paleosol, respectively).

#### 4. Discussion

Although loess has the same material source as paleosol, their distinct sedimentary environments contribute to discrepancies in soil texture, so that the basic physical indexes and shear behavior of loess are distinct from those of paleosol.  $\text{CaCO}_3$  is well-preserved in loess strata, while the amount of  $\text{CaCO}_3$  preserved in paleosol strata is relatively small because intense eluviation results in the enrichment of  $\text{CaCO}_3$  in the form of calcareous concretions at the bottom of the paleosol layer [44,45]. This provides support for the finding that the content of carbonate minerals in loess was greater than that in the paleosol. The superior shear strength and strength parameters in the paleosol can, therefore, be attributed to the presence of calcareous concretions, playing a skeletal role. Furthermore, the greater clay contents and carbonate minerals in the paleosol (Tables 1 and 2) evidence that there are stronger cementation bonds in the paleosol, which make a heavy contribution to its shear properties [46]. Similar conclusions were discovered in the literature [47]. Different from our research, in previous studies, it was found that the internal friction angle of the paleosol was slightly smaller than that of the loess. This may be since the paleosol layer was compared with the underlying loess layer, while the loess layer in our article overlay the paleosol layer.

The underlying mechanism of the reduction in shear strength by water is a weakening of the cementation bonds between particles. The thickness of the water film between soil particles gradually increases with a higher initial moisture content, resulting in a greater strength loss created by bound water [48]. In other words, the aggregate size of soils gradually enlarges with an increasing initial moisture content, and inter-aggregate pores are filled with free water, which ultimately causes a decrease in shear strength [49]. From another point of view, the partial clay minerals and soluble carbonate minerals that play a cementing role in soil are dissolved by excess water, reducing the bonding strength

(mainly cementation and Van der Waals force) between soil particles [50,51]. Therefore, there is a negative correlation between shear strength and the moisture content. To sum up, cohesion is the most crucial factor impacting shear strength. Since the paleosol is deposited under warm and moist climatic conditions, the solidified cohesive force generated by cementitious material between particles is stronger than that of loess, and as a consequence, the paleosol's cohesion remarkably outweighs that of loess. The influence of the internal friction angle—contributed by the sliding friction of the particle surface and the interlocking force between particles—on shear strength is limited. A variation in moisture content does not change the surface roughness of loess and paleosol particles, so the reduction in their internal friction angle is barely significant.

## 5. Conclusions

Conventional direct shear tests were implemented to investigate the shear behavior of undisturbed loess and paleosol with distinct initial moisture contents under various normal stresses. The SWCCs of loess and paleosol samples were measured separately and used to predict their unsaturated shear strength formulas. On the basis of this work, the following conclusions can be drawn:

- There are significant discrepancies in basic physical properties between loess and paleosol samples, particularly in natural moisture content, Atterberg limit, grain size distribution, and mineral composition.
- As the initial moisture content and normal stress increase, different shapes of shear stress–shear displacement curves for loess and paleosol are observed, and their shear failure behavior gradually transitions from strain softening to strain hardening. The strain softening phenomenon of loess samples at a low initial moisture content is not as significant as that of paleosol samples under the same conditions.
- The shear strength of loess and paleosol samples is negatively correlated with an increased initial moisture content and decreased normal stress. The sensitivity of the internal friction angle to water is much less than that of the cohesion. There is an exponentially decreasing relationship between cohesion and an increased initial moisture content, while the internal friction angle shows a decreasing trend with a limited attenuation range, along with augmenting the initial moisture content. This is close to the weakening action of water on soil's inter-particle cementation.
- On the basis of the Vanapalli model, formulas for predicting the unsaturated shear strengths of undisturbed loess and paleosol were put forward respectively. The applicability of the prediction models proposed in this paper and the accuracy of their fitting parameters were verified by using experimental data.
- This study has offered scientific guidance on how we should understand the mechanism of loess landslides in the South Jingyang tableland. However, due to the size and boundary effects of our indoor experiments, further in situ direct shear tests can more accurately reflect the shear characteristics of undisturbed, unsaturated loess and paleosol.

**Author Contributions:** Conceptualization, F.D. and Z.H.; data curation, P.L. and J.W.; formal analysis, P.L.; funding acquisition, Z.H. and P.L.; methodology, P.L. and F.D.; writing—original draft preparation, P.L.; writing—review and editing, F.D. and Z.H. All authors have read and agreed to the published version of the manuscript.

**Funding:** This research was financially supported by the Key Research and Development Project of Henan Province (No. 22111321500) and the Ph.D. Student Innovation Fund of the North China University of Water Resource and Electric Power (No. NCWUBC202235).

**Institutional Review Board Statement:** Not applicable.

**Informed Consent Statement:** Not applicable.

**Data Availability Statement:** Data are contained within the article.

**Conflicts of Interest:** The authors declare no conflicts of interest.

## References

- Derbyshire, E.; Dijkstra, T.A.; Smalley, I.J.; Li, Y. Failure mechanisms in loess and the effects of moisture content changes on remoulded strength. *Quat. Int.* **1994**, *24*, 5–15. [[CrossRef](#)]
- Svirčev, Z.; Nikolić, B.; Vukić, V.; Markovic, S.B.; Gavrilov, M.B.; Smalley, I.J.; Obreht, I.; Vukotic, B.; Meriluoto, J. Loess and life out of Earth? *Quat. Int.* **2016**, *399*, 208–271. [[CrossRef](#)]
- Lehmkuhl, F.; Zens, J.; Krauß, L.; Schulte, P.; Kels, H. Loess-paleosol sequences at the northern European loess belt in Germany: Distribution, geomorphology and stratigraphy. *Quat. Sci. Rev.* **2016**, *153*, 11–30. [[CrossRef](#)]
- Liu, T.S. *Loess and the Environment*; Science Press: Beijing, China, 1985.
- Li, Y.R.; Shi, W.H.; Aydinb, A.; Beroya-Eitnerc, M.A.; Gao, G.H. Loess genesis and worldwide distribution. *Earth-Sci. Rev.* **2020**, *201*, 102947. [[CrossRef](#)]
- Wei, X.; Hattab, M.; Taibi, S.; Bicalho, K.V.; Xu, L.; Fleureau, J.M. Crack development and coalescence process in drying clayey loess. *Geomech. Eng.* **2021**, *25*, 535–552. [[CrossRef](#)]
- Zhou, Y.F.; Tham, L.G.; Yan, R.W.M.; Xu, L. The mechanism of soil failures along cracks subjected to water infiltration. *Comput. Geotech.* **2014**, *55*, 330–341. [[CrossRef](#)]
- Wang, G.L.; Li, T.L.; Xing, X.L. Research on loess flow-slides induced by rainfall in July 2013 in Yan’an, NW China. *Environ. Earth Sci.* **2015**, *73*, 7933–7944. [[CrossRef](#)]
- Ma, P.H.; Peng, J.B.; Wang, Q.Y.; Duan, Z.; Meng, Z.J.; Zhuang, J.Q. Loess landslides on the South Jingyang Platform in Shaanxi Province, China. *Q. J. Eng. Geol. Hydrogeol.* **2019**, *52*, 547–556. [[CrossRef](#)]
- Zhao, K.Y.; Xu, Q.; Liu, F.Z.; Xiu, D.H.; Ren, X.H. Field monitoring of preferential infiltration in loess using time-lapse electrical resistivity tomography. *J. Hydrol.* **2020**, *591*, 125278. [[CrossRef](#)]
- Zhang, J.W.; Mu, Q.Y.; Garg, A.; Liu, F.L.; Cao, J. Shear behavior of unsaturated intact and compacted loess: A comparison study. *Environ. Geol.* **2020**, *79*, 79. [[CrossRef](#)]
- Yao, Y.G.; Zhang, Y.C.; Gao, X.L.; Huang, H.W.; Liu, D.F.; Hui, X.Q. Study on permeability and collapsibility characteristics of sandy loess in northern Loess Plateau, China. *J. Hydrol.* **2021**, *603*, 126883. [[CrossRef](#)]
- Sun, P.P.; Zhang, M.S.; Jia, J.; Cheng, X.J.; Zhu, L.F.; Xue, Q.; Wang, J.Y. Geo-hazards research and investigation in the loess regions of Western China. *Northwestern Geol.* **2022**, *55*, 96–107. [[CrossRef](#)]
- Duan, Z.; Cheng, W.C.; Peng, J.B.; Wang, Q.Y.; Chen, W. Investigation into the triggering mechanism of loess landslides in the south Jingyang platform, Shaanxi province. *Bull. Eng. Geol. Environ.* **2019**, *78*, 4919–4930. [[CrossRef](#)]
- Peng, D.L.; Xu, Q.; Zhang, X.L. Hydrological response of loess slopes with reference to widespread landslide events in the Heifangtai terrace, NW China. *J. Asian Earth Sci.* **2019**, *171*, 259–276. [[CrossRef](#)]
- Tan, C.X.; Sun, W.F.; Meng, J.; Zhang, C.S.; Wu, S.R.; Shi, J.S.; Li, B.; Wang, T. Research on loess-paleosol engineering geology features from the borehole cores of a typical section in Baoji area, Shaanxi province, China. *Environ. Earth Sci.* **2015**, *74*, 4469–4491. [[CrossRef](#)]
- Zhong, Z.L.; Liu, Y.X.; Liu, X.R.; Li, X.Y.; Wang, S. Influence of moisture content on shearing strength of unsaturated undisturbed quaternary system middle Pleistocene. *J. Cent. South Univ.* **2015**, *22*, 2776–2782. [[CrossRef](#)]
- Gao, B.L.; Su, L.L. Triaxial mechanical testing of undisturbed unsaturated loess. *Soil Mech. Found. Eng.* **2020**, *57*, 57–64. [[CrossRef](#)]
- Lian, B.Q.; Peng, J.B.; Wang, X.G. Moisture content effect on the ring shear characteristics of slip zone loess at high shearing rates. *Bull. Eng. Geol. Environ.* **2020**, *70*, 999–1008. [[CrossRef](#)]
- Nan, J.J.; Peng, J.B.; Zhu, F.J.; Ma, P.H.; Liu, R.; Leng, Y.Q.; Meng, Z.J. Shear behavior and microstructural variation in loess from the Yan’an area, China. *Eng. Geol.* **2021**, *280*, 105964. [[CrossRef](#)]
- Pu, X.W.; Wan, L.M.; Wang, P. Initiation mechanism of mudflow-like loess landslide induced by the combined effect of earthquakes and rainfall. *Nat. Hazards.* **2021**, *105*, 3079–3097. [[CrossRef](#)]
- Yang, Z.Q.; Chen, M.; Zhang, J.; Ding, P.; He, N.; Yang, Y. Effect of initial water content on soil failure mechanism of loess mudflow disasters. *Front. Ecol. Evol.* **2023**, *11*, 1141155. [[CrossRef](#)]
- Hadzi-Nikovic, G.; Coric, S.; Caki, L. Effect of initial conditions on strength of unsaturated compacted loess soil. *Gradevinar* **2014**, *66*, 225–235. [[CrossRef](#)]
- Yates, K.; Russell, A.R. The unsaturated characteristics of natural loess in slopes, New Zealand. *Géotechnique* **2023**, *73*, 871–884. [[CrossRef](#)]
- Lu, H.; Jia, J.; Wang, Y.J.; Yin, Q.Z.; Xia, D.S. The cause of extremely high magnetic susceptibility of the S5S1 paleosol in the central Chinese Loess Plateau. *Quatern. Int.* **2018**, *493*, 252–257. [[CrossRef](#)]
- Chen, J.; Stevens, T.; Yang, T.B.; Qiang, M.R.; Matishov, G.; Konstantinov, E.; Kurbanov, R.; Zeng, B.; Shi, P.H. Revisiting Late Pleistocene Loess-Paleosol Sequences in the Azov Sea Region of Russia: Chronostratigraphy and Paleoenvironmental Record. *Front. Earth Sci.* **2022**, *9*, 808157. [[CrossRef](#)]
- Zykina, V.S.; Zykina, V.S.; Volvakh, A.O.; Radakovic, M.G.; Gavrilov, M.B.; Markovic, S.B. Late Pleistocene loess-paleosol sequence at the Belovo section, south of Western Siberia, Russia: Preliminary results. *Quatern. Int.* **2022**, *620*, 75–84. [[CrossRef](#)]
- Yuan, W.N.; Fan, W.; Jiang, C.C.; Peng, X.L. Experimental study on the shear behavior of loess and paleosol based on ring shear tests. *Eng. Geol.* **2019**, *250*, 11–20. [[CrossRef](#)]

29. Fredlund, D.G.; Rahardjo, H. *Soil Mechanics for Unsaturated Soil*; Wiley: New York, NY, USA, 1993.
30. Zhai, Q.; Rahardjo, H.; Satyanaga, A.; Dai, G.L. Estimation of unsaturated shear strength from soil-water characteristic curve. *Acta Geotech.* **2019**, *14*, 1977–1990. [[CrossRef](#)]
31. Cai, G.Q.; Zhang, C.; Huang, Z.W.; Li, J.L.; Hou, J.L. Experimental study on influences of moisture content on shear strength of unsaturated loess. *Chin. J. Geotech. Eng.* **2020**, *42*, 32–36. [[CrossRef](#)]
32. Jiang, T.; Zhao, J.D.; Zhang, J.R.; Wang, L.J.; Song, C.Y.; Zhai, T.Y. Hydromechanical behavior and prediction of unsaturated loess over a wide suction range. *Geomech. Eng.* **2021**, *26*, 275–288. [[CrossRef](#)]
33. Duan, Z.; Li, W.K.; Wang, Q.Y. Types and spatial-temporal distribution of loess landslides in the south plateau of lower Jing River. *J. Xi'an Sci. Tech. Univ.* **2015**, *35*, 369–375. [[CrossRef](#)]
34. Lei, X.Y. *The Cause of Formation, Prevention and Cure of Geological Disasters of Loess*, 1st ed.; Peking University Press: Beijing, China, 2014.
35. Wang, Z.X. The Loess Plateau Region-Encyclopedia of World Geographic Data Entry. *J. Glob. Chang. Data Discov.* **2017**, *1*, 113. [[CrossRef](#)]
36. Wang, J.D.; Li, P.; Ma, Y.; Vanapalli, S.K.; Wang, X.G. Change in pore-size distribution of collapsible loess due to loading and inundating. *Acta Geotech.* **2020**, *15*, 1081–1094. [[CrossRef](#)]
37. Standardization Administration of China (SAC), Ministry of Water Resources. *China National Standards GB/T50123-2019, Standard for Soil Test Method*; China Planning Press: Beijing, China, 2019.
38. Nam, S.; Gutierrez, M.; Diplas, P.; Petrie, J. Determination of the shear strength of unsaturated soils using the multistage direct shear test. *Eng. Geol.* **2011**, *122*, 272–280. [[CrossRef](#)]
39. Tang, C.; Borden, R.; Gabr, M. A Simplified Direct Shear Testing Procedure to Evaluate Unsaturated Shear Strength. *Geotech. Test J.* **2018**, *41*, 223–234. [[CrossRef](#)]
40. Gao, Z.A.; Li, P.; Xiao, J.J.; Li, T.L. Evaluation of shear strength of unsaturated loess using conventional direct shear test. *J. Eng. Geol.* **2020**, *28*, 344–351. [[CrossRef](#)]
41. Oloo, S.Y.; Fredlund, D.G. A method for determination of  $\varphi^b$  for statically compacted soils. *Can. Geotech. J.* **1996**, *33*, 272–280. [[CrossRef](#)]
42. Lin, H.Z.; Li, G.X.; Yu, Y.Z.; Lü, H. Influence of matric suction on shear strength behavior of unsaturated soils. *Rock Soil Mech.* **2007**, *28*, 1931–1936. [[CrossRef](#)]
43. Vanapalli, S.K.; Fredlund, D.G.; Pufahl, D.E.; Clifton, A.W. Model for the prediction of shear strength with respect to soil suction. *Can. Geotech. J.* **1996**, *33*, 379–392. [[CrossRef](#)]
44. Zhao, J.B.  $\text{CaCO}_3$  and sedimentary environment of loess strata. *Acta Seismol. Sin.* **1993**, *11*, 136–142. [[CrossRef](#)]
45. Wang, L.Q.; Wang, Z.Q.; Xin, F.; Li, K.Y.; Li, S.; Hu, X.Y. Strength and structure of  $Q_3$  paleosol. *Chin. J. Geotech. Eng.* **2021**, *43*, 209–213. [[CrossRef](#)]
46. Zhu, J.H.; Zhang, H.Y.; Wang, Z.M. Physico-mechanical properties of thick paleosol in  $Q_1$  strata of the Chinese Loess Plateau and their variations during tunnel excavation. *Eng. Geol.* **2021**, *295*, 106426. [[CrossRef](#)]
47. Zhu, J.H.; Zhang, H.Y.; Yang, S.Q.; Wang, T.T.; Zhou, G.P. Physico-mechanical properties of loess-paleosol sequence from  $Q_4$  to  $Q_1$  strata in the Chinese Loess Plateau. *Bull. Eng. Geol. Environ.* **2022**, *81*, 416. [[CrossRef](#)]
48. Ye, C.; Guo, Z.L.; Cai, C.F.; Wang, J.G.; Deng, J. Effect of water content, bulk density, and aggregate size on mechanical characteristics of Aquults soil blocks and aggregates from subtropical China. *J. Soils Sediments* **2017**, *17*, 210–219. [[CrossRef](#)]
49. Yuan, K.Z.; Ni, W.K.; Lü, X.F.; Wang, H.M. Effect of water distribution on shear strength of compacted loess. *Geomech. Eng.* **2022**, *31*, 519–527. [[CrossRef](#)]
50. Li, P.; Xie, W.L.; Pak, R.Y.S.; Vanapalli, S.K. Microstructural evolution of loess soils from the loess plateau of China. *Catena* **2019**, *173*, 276–288. [[CrossRef](#)]
51. Wei, Y.N.; Fan, W.; Fu, C.B.; Yu, B. Experimental Investigation of the Hydration Swelling Effect of Clay Minerals on Loess Collapsibility. *Int. J. Geomech.* **2023**, *23*, 06022036. [[CrossRef](#)]

**Disclaimer/Publisher's Note:** The statements, opinions and data contained in all publications are solely those of the individual author(s) and contributor(s) and not of MDPI and/or the editor(s). MDPI and/or the editor(s) disclaim responsibility for any injury to people or property resulting from any ideas, methods, instructions or products referred to in the content.